Performance Study on Cathode Microporous Layer Using Biomass Activated Carbon for Passive Direct Ethanol Fuel Cell

Panuwat Ekdharmasuit[1*], Jiratchaya Sapkitjakarn[1], Phuritutphong Sangwanangkool[1], Akarasingh Bampenrat[1], Hussanai Sukkathanyawat[1]

[1] Faculty of Science Energy and Environment, King Mongkut's University of Technology North Bangkok (Rayong Campus), Rayong, 21120, Thailand

* Corresponding author's email address: panuwat.e@sciee.kmutnb.ac.th

ABSTRACT

In passive direct ethanol fuel cells (DEFCs), the micro-porous layer (MPL) is a vital component of the membrane electrode assembly (MEA), facilitating gas-liquid mass transport and improving electronic conductivity. The conducted study involved preparing various carbon materials for the cathode MPL, including Ketjen Black (KB), activated carbon (AC) from Durian shells, and a 15% weight mixture of AC and KB (AC15%). Characterization of the activated carbon was carried out using nitrogen adsorption-desorption isotherm analysis. Additionally, various electrochemical techniques, including cell polarization, electrochemical impedance spectroscopy (EIS), anode half-cell polarization, and anode EIS, were conducted to examine the effects of the cathode MPLs on cell performance. The results indicated that the cell with the conventional KB cathode MPL displayed the highest performance, whereas the AC15% and AC cathode MPLs showed relatively lower performances, respectively. The AC cathode MPL in the cell encountered challenges, such as decreased pore volume, increased micropores, and a hydrophobic electrode nature, leading to reduced gas transport resulting in poor cell performance. In contrast, the AC15% cathode MPL, which combined AC and KB in the electrode, achieved an appropriate micropore and mesopore balance. However, performance did not improve due to a heterogeneous contact surface between the cathode catalyst layer and the cathode MPL, resulting in higher ohmic resistance. Incorporating biomass-based materials into the electrode presents an interesting possibility due to the utilization of cheap and readily available precursors, as well as the ability to tailor morphology. Conducting a systematic study of durian shell activated carbons would reveal improved properties of the carbon material suitable for implementing in the MPL of passive DEFCs.

Keywords: direct ethanol fuel cell, Passive fuel cell, activated carbon, microporous layer, electrochemical impedance spectroscopy.

INTRODUCTION

Direct alcohol fuel cells (DAFCs) have generated considerable interest as a promising alternative for powering portable devices. These fuel cells operate by directly converting chemical energy into electricity through a redox reaction between the liquid fuel and the oxidant [Elsaid et al. 2021]. Among the various DAFCs, direct methanol fuel cells (DMFCs) have garnered significant attention due to the remarkable properties of methanol fuel. However, it is important to note that methanol poses inherent risks of toxicity to humans as well as exhibits high volatility and flammability [Oliveira et al., 2017]. Ethanol has emerged as a favorable and compelling fuel choice for DAFCs. It offers reduced toxicity, plentiful accessibility from sustainable sources, and a substantial energy density per unit weight [Shaari et al., 2020]. Consequently, direct ethanol fuel cells (DEFCs) have been introduced as another promising power source with significant commercialization potential.

DEFCs are commonly divided into two categories: active and passive, based on their operational concept [Pereira et al., 2014]. In the active concept, the cell relies on an external power source to activate an additional component that supplies

fuel and oxidant to the cell. Extensive research in recent years has focused on active DEFCs, particularly in the development of advanced electrocatalysts to enhance the ethanol oxidation reaction (EOR) [Wang et al., 2021] and Nafion-based composite membranes to improve proton conductivity as well as reduce fuel permeability [Matos et al., 2020], modeling of cell performance, anode polarization, and product distribution [Monreal et al., 2019; Pittayaporn et al., 2019], and the design of mass transfer within the membrane electrode assembly (MEA), with emphasis on the microporous layer (MPL) [Ekdharmasuit et al., 2013; Yong et al., 2020]. On the other hand, the passive concept utilizes natural forces like capillary action, diffusion, convection, and evaporation to facilitate the fuel and oxidant supply, eliminating the need for external power. This passive concept offers several advantages, such as reduced system volume, lower product cost, and increased power density [Cao et al., 2010]. Only a limited number of studies have been conducted so far in the current research on passive DEFCs. Previous research efforts have primarily focused on exploring the influence of various factors, including operating parameters [Pereira et al., 2014; Azam et al., 2019], fuel permeability, working parameters [Shrivastava et al. 2019], modifications to the MEA structure [Moreno et al., 2015], and performance modeling affect the overall cell performance [Oliveira et al., 2017].

On the basis of previous works performed with passive DMFC, one of the primary concerns is the mass transfer behavior within the cathode diffusion layer. This issue arises at the cathode, because the air supply relies solely on natural forces and water is produced by oxygen reduction reaction. Therefore, the cathode diffusion layer plays a crucial role in enhancing oxygen transfer and minimizing water accumulation, leading to improved cell performance. In recent times, researchers have conducted extensive investigations into the mass transport associated with the customized microporous layer (MPL), particularly at the cathode electrode in passive DMFCs. The MPL, located between the catalyst layer and backing layer and composed of carbon powder and binder, plays a vital role in regulating fuel and reactant transport, as well as facilitating water removal and diffusion. In a notable study by Cao et al. [Cao et al., 2010], a novel membrane electrode assembly (MEA) was designed by introducing a double MPL specifically for the cathode. This innovative approach involved the utilization of appropriate carbon materials for the MPL, resulting in a faster rate of oxygen transfer and a slower crossover of water from the anode to the cathode. These advancements led to higher performance and greater stability in the system. Zhang et al. [Zhang et al., 2011] conducted a study to assess how the polytetrafluoroethylene (PTFE) content in the cathode diffusion layer affects the performance of passive DMFCs. Their findings revealed that a cathode diffusion layer with 40% PTFE is considered the ideal composition for achieving effective long-term water management. Cao et al. [Cao et al., 2014] introduced a new cathode MPL for passive DMFCs using a porous carbon material with uniform mesopores and a high pore volume. This innovative MPL design significantly improved performance and stability, attributed to enhanced oxygen transfer rate and improved water back diffusion. Braz et al. [Braz et al., 2019] examined the impact of cathode MPL and backing layer properties on the power output of passive DMFCs using commercially available materials. The findings revealed that thinner carbon cloth yielded the highest performance, attributed to its increased porosity, facilitating enhanced oxygen diffusion and improved water management within the cell.

The significance of employing carbon powder material in the formation of the desired MPL to facilitate efficient management of mass transfer is acknowledged in the literature. Vulcan XC72 and Ketjen Black (KB) are commonly employed as carbon materials in the MPL due to their appropriate pore structure and electrical conductivity. Recently, researchers have developed activated carbons (AC) with a diverse range of pore characteristics and surface areas by utilizing various biomass sources. These AC materials are specifically designed for application in electrochemical devices, such as electric double-layer capacitors (EDLCs) and DMFCs. For instance, Tey et al. [Tey et al., 2016] synthesized AC from durian shells using chemical activation methods to create a cost-effective electrode material for EDLCs. The resulting AC material exhibited a high surface area and mesoporous structure, leading to comparable and highly stable capacitance in the EDLC. In another study, Balakrishnan et al. [Balakrishnan et al., 2017] prepared AC from factory waste-tea to be used as the cathode MPL in an active DMFC. The electrode composition containing 15% AC along with KB demonstrated

superior performance due to the reduction of mass transfer resistance facilitated by the appropriate pore structure, particle size characteristics, and the presence of a cracked structure. Significant advancements in carbon material utilization provide promising opportunities for enhancing mass transfer management and optimizing the performance of electrochemical devices. Thus, there is potential in utilizing abundant and affordable biomass wastes as raw materials to produce porous carbons for various electrochemical applications.

Passive DEFC exhibits notable distinctions in mass transport behavior compared to passive DMFCs. These differences could be attributed to variations in reactant molecular weight and kinetics rates of ethanol reactions on both the anode and cathode catalysts [Ong et al., 2017], leading to different management strategies for ethanol and water transport. Consequently, studying the effect of mass transport, particularly at the cathode, poses one of the most challenging issues in understanding passive DEFC performance. According to the author's understanding, there is only one available experimental study on the cathode electrode of passive DEFCs, conducted by Moreno-Jiménez et al. [Moreno et al., 2015]. Investigating the effects of oxygen transport at the cathode on cell performance was the main goal of their study. However, limited research attention has been directed towards mass transport management in passive DEFC. In the conducted research, the authors aimed to prepare different carbon materials for the cathode MPL in passive DEFC. This involved the utilization of conventional KB, AC, and a composite mixture of AC and KB with a weight percentage of 15% (AC15%). AC was synthesized from durian shells to apply as a carbon material. The nitrogen adsorption-desorption isotherm technique was employed to characterize the prepared activated carbon. Furthermore, various characterization techniques, such as cell polarization, cell electrochemical impedance spectroscopy (EIS), and anode EIS, were employed to assess the influence of the cathode MPLs on the performance of the cell.

MATERIALS AND METHOD

Preparation of activated carbon

Activated carbon was produced using durian shells, following the process reported in previous work [Tey et al., 2016]. The durian shells were washed before being impregnated with a chemical solution of 1.0 M phosphoric acid (H_3PO_4) at a mass to volume ratio of 1:25. The combination was agitated for 24 hours, and then the water was removed by heating the mixture for another 24 hours at 110 °C. Next, the sample was carbonized at 700 °C for 1 hour with a heating rate of 10 °C·min^{-1} under a nitrogen atmosphere. The final product was washed with 0.1 M hydrochloric acid and de-ionized water. Finally, the sample was dried in an oven at 110 °C for 24 hours. Nitrogen adsorption-desorption isotherms and pore size distribution analysis techniques were performed using the V-Sorb 2800P Surface Area and Porosimetry Analyzer equipment. The Brunauer-Emmett-Teller (BET) method was used to determine the total surface area using the isotherm data.

Membrane electrode assembly fabrication

The backing layers (BL) for both the anode and cathode were made of carbon cloth (Type A, no wet-proofed, E-TEK). In the case of the anode MPL, a mixture comprising Vulcan carbon and Nafion ionomer was applied onto the anode BL. This mixture consisted of 20 wt.% Nafion and had a carbon loading of 2 mg·cm^{-2}. Simultaneously, the cathode MPL was developed by coating the slurry containing the desired carbon material and Nafion ionomer onto the cathode BL. This slurry also included 20 wt.% Nafion and had a carbon loading of 2 mg·cm^{-2}. Different carbon materials were employed for the cathode MPL, including conventional Ketjen Black (KB), activated carbon (AC), and a mixture of activated carbon and Ketjen Black with a weight percentage of 15% (AC15%). AC15% was suggested to optimize the gas transfer rate and improve water removal in DMFC [Balakrishnan et al., 2017].

Pt-Sn (3:1 a/o) on Vulcan XC72 carbon (Johnson Matthey), the 5wt% Nafion ionomer solution (Sigma-Aldrich), and isopropyl alcohol were combined in an ultrasonic bath for an hour to create the anodic catalyst ink. The anode catalyst layer (CL), which was created by coating the ink solution onto the anode MPL, was then dried for one hour in an oven at 80 °C. The resulting anode catalyst layer had a metal loading of 2 mg·cm^{-2} and a Nafion ionomer loading of 20 wt.% relative to the dry catalyst layer. The cathode CL was prepared following the identical procedure used for the anode catalyst layer. The resulting cathode
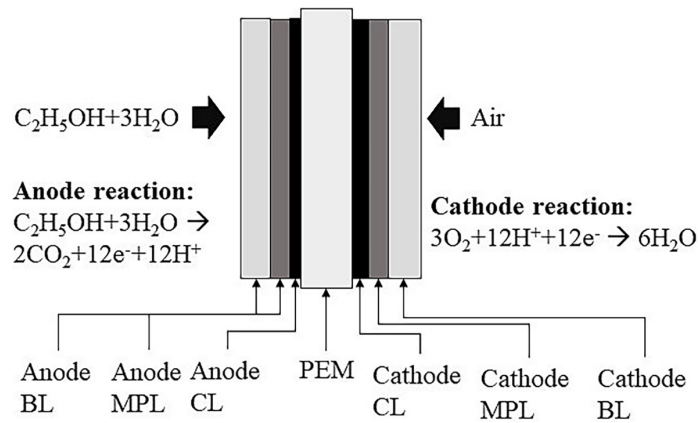
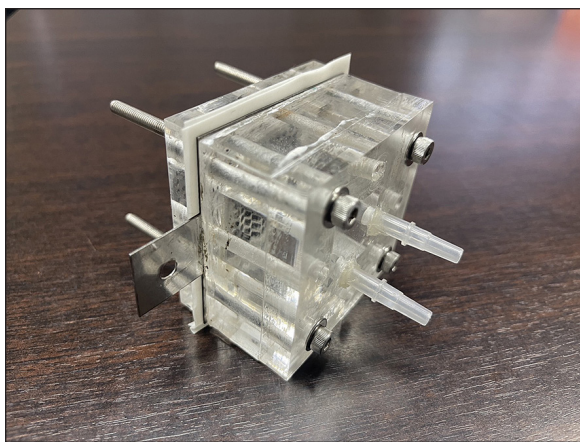**Figure 1.** A schematic representation of the component of the membrane electrode assembly (MEA) in the DEFC

Figure 2. In-house fuel cell stack

CL had a metal loading of 1 mg·cm^{-2} (Pt/C, E-TEK) and a Nafion ionomer loading of 20 wt.% of the dry catalyst layer. The active area for both sides was 5 cm^2. The proton exchange membrane (PEM) used in the experiment was Nafion® 115, provided by Dupont. To prepare the membrane, three primary procedures were followed: initial cleaning using a 3% H_2O_2 solution, subsequent boiling in a 0.5 M H_2SO_4 solution, and final rinsing with de-ionized water. The same conditions of 70 °C for 1 hour were applied to each process. The MEA was built with anode and cathode electrodes on either side of the Nafion membrane. A schematic illustration of the MEA parts is shown in Figure 1. Afterward, the MEA underwent compression between two acrylic blocks and was subsequently integrated into the in-house fuel cell stack, as shown in Figure 2.

Fuel cell characterization

The performance and characterization data were acquired using a Potentiostat/Galvanostat device (Metrohm Autolab, PGSTAT 302N, Utrecht, The Netherlands). Figure 3 presents an illustration of the apparatus configuration. In order to establish a consistent and stable cell performance, a single cell was activated and operated continuously for a period of 4 hours. The anode was supplied with an ethanol solution at a flow rate of 1 ml·min^{-1} and a concentration of 1 M, while the cathode utilized ambient air at room temperature and atmospheric pressure. Fuel cell polarization measurements were performed in potentiodynamic polarization mode, covering a range from the open circuit voltage (OCV) down to 0.1 V. Data points were gathered at intervals of 10 seconds during the measurements, which were carried out at a scan rate of 10 mVs^{-1}. MEA ohmic and reaction resistances were determined through EIS measurements recorded in a potentiostatic mode at 0.3 V. The amplitude was set at 30 mV,
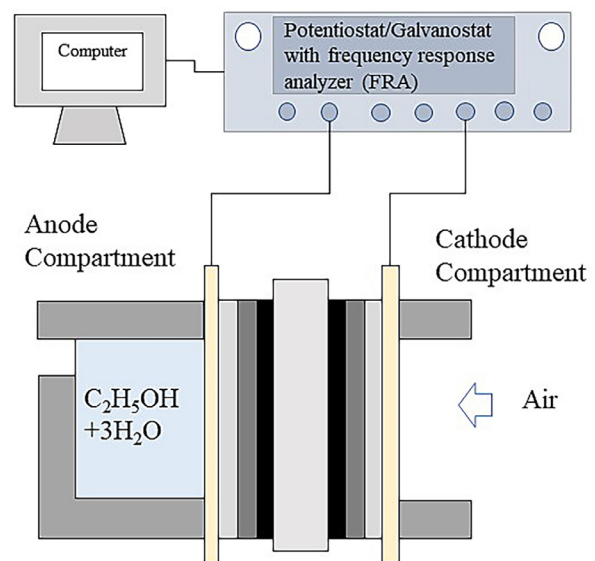

Figure 3. An illustration of the equipment setup

and the frequency range was 5 kHz to 0.05 Hz with 10 points per decade. Within the impedance spectra of the full-cell measurement, the anode was utilized as the working electrode (WE) with an ethanol solution, while the cathode served the dual roles of reference electrode (RE) and counter electrode (CE), being exposed to ambient air. On the other hand, in the half-cell anode impedance spectra, the anode also employed ethanol solution as the working electrode (WE), while the cathode utilized hydrogen gas at a flow rate of 100 ml·min^{-1}, serving as both the dynamic hydrogen electrode (DHE) and counter electrode (CE), as suggested in a literature [Prabhuram et al. 2010].

RESULTS AND DISCUSSION

Characterization of the activated carbon

Figure 4 shows the nitrogen adsorption-desorption isotherm of AC, indicating a pore volume of approximately 1.39 cm^3·g^{-1} and a BET surface area of 1,036 m^2·g^{-1}. In comparison, KB had a higher pore volume (1.79 cm^3·g^{-1}) and a lower BET surface area (750 m^2·g^{-1}). Figure 5 depicts the pore size distribution of AC, revealing that the sample consists of 72.66% mesopores and 27.34% micropores, while KB carbon had 84.36% mesopores and 15.64% micropores. Notably, AC exhibited a greater volume of micropores than KB. These findings are summarized in Table 1. It has been suggested that carbon containing sufficient micro/mesopores could offer good mass transport across the electrode, leading to an improvement in cell performance [Hiramitsu et al. 2010; Cao et al. 2014; Balakrishnan et al. 2017]. The mesopore could serve as a channel for water transport, while both meso- and micropores are suitable for gas transport [Weber et al. 2005]. As a result, KB would experience air mass transport losses because of the limited presence of micropores in the cathode diffusion layer. On the other hand, a greater proportion of micropores in the AC sample could enhance water removal in the cathode. However, in the conducted work, some disadvantages of the cell with an AC cathode MPL were discovered, which led to lower cell performance. These drawbacks were discussed in the next section.

Fuel cell performance

The polarization and power density curves of passive DEFCs with the conventional (KB), AC, and AC15% cathode MPL employing a 4 M ethanol solution at 25 °C are illustrated in Figure 6. These three cells exhibited different performances throughout the entire region. The maximum
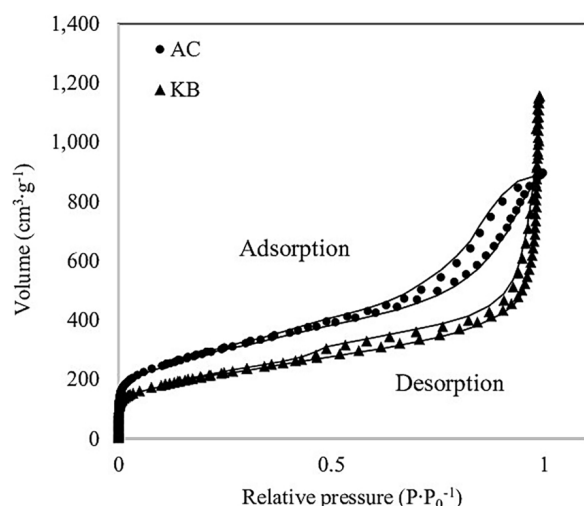
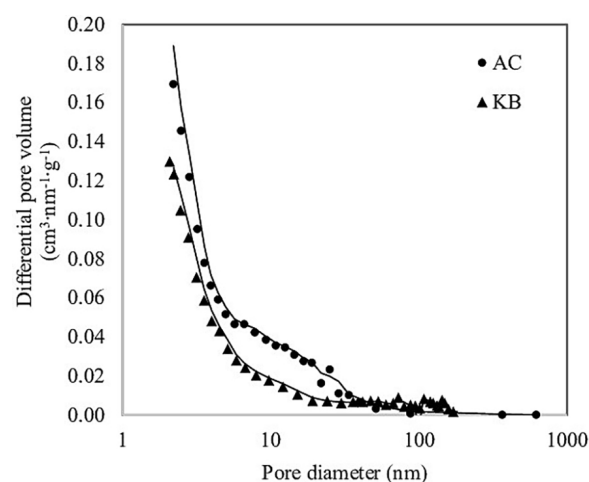**Figure 4.** Nitrogen adsorption-desorption isotherm of AC and KB

Figure 5. Pore size distribution of AC and KB

Table 1. Surface area and pore properties of synthetic activated carbon (AC) and Ketjen Black (KB)

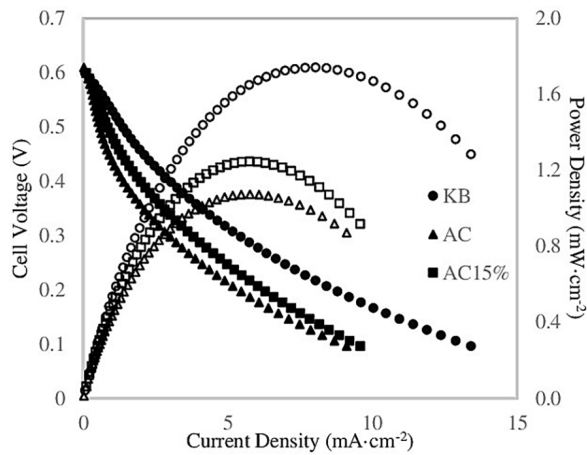| Sample	Specific surface area (m^2·g^{-1})	Total pore volume[a] (cm^3·g^{-1})	Micropore volume[b] (cm^3·g^{-1})	Mesopore volume[c] (cm^3·g^{-1})	Microporosity (%)	Mesoporosity (%)
AC	1036	1.39	0.38	1.01	27.34	72.66
KB	750	1.79	0.28	1.51	15.64	84.36

Figure 6. Polarization curves for three passive DEFCs with the KB, AC and AC15% cathode diffusion layer, respectively, at a 4 M ethanol solution and 25 °C

power density for the AC cathode MPL was 1.074 mW·cm^{-2}, which was lower than that of the KB and AC15% cathode MPL (1.741 and 1.246 mW·cm^{-2}, respectively). Obviously, the middle and high current density regions exhibited a noticeable difference in cell performance. Therefore, the utilization of carbon materials with different cathode MPLs could influence both the ohmic and mass transport regions. This result confirms the previous DMFC research [Balakrishnan et al. 2017], which found that the AC cathode MPL resulted in lower cell performance due to lower electrical conductivity of AC. However, the contradictory finding was that the cell performance did not improve with the use of the AC15% cathode MPL. It was believed that the potential benefits of increasing the proportion of micropores by incorporating AC in the cell with AC15% cathode MPL were hindered by unsuitable cathode MPL morphology. The impact of the cathode structure and morphology of cathode MPLs was later discussed through electrochemical measurements conducted on both the full cell and anode half-cell.

Electrochemical measurement

To identify the resistance mechanism, in-situ EIS was conducted on the full cells, and the corresponding impedance spectra (Nyquist plots by EIS) for the three passive DEFCs were analyzed, as shown in Figure 7a. The acquired EIS data were further analyzed by fitting them to a modified equivalent circuit, which was adapted from established models [Cao et al. 2010; Cao et al.

2014], as illustrated in Figure 7b. The meanings of each parameter are explained as follows: L represents the inductance generated by the conducting cables of the equipment, while W represents the Warburg component. R_{ohm} corresponds to the ohmic resistance of the cell. R_A and R_C denote the charge transfer resistance of the anode and cathode electrodes, respectively. CPE$_A$ and CPE$_C$ capture the capacitive behavior that represents the roughness and non-uniformity of the anode and cathode electrodes, respectively. Table 2 displays the fitting parameters, and the chi-square (χ^2) values for these simulations was approximately 0.03 to 0.05, which was in close agreement with the authors' previous work by the ($\chi^2 = 0.03$) [Ekdharmasuit et al. 2014], indicating a strong correlation between the equivalent circuit model and the experimental results. The result presented that R_{ohm} of the cell with AC15% cathode MPL (0.9818 Ω) was higher compared to both KB (0.7175 Ω) and AC (0.6974 Ω) cathode MPLs. This observation indicates that the ohmic resistance of the KB and AC cathode MPLs was relatively similar, while the AC15% cathode MPL exhibited significantly higher ohmic resistance (40.78% increased) due to its increased electronic conductivity. The addition of AC to the KB carbon material was believed to result in a distinct chemical structure, varied particle size, and morphology, as well as changes in hydrophobicity of the electrode. These factors contributed to the development of surface cracks, as discussed in the literature [Balakrishnan et al. 2017], which resulted in reduced surface contact and diminished electronic conductivity within the cathode electrode.

The analysis of the R$_C$ regarding the kinetics reaction resistance of the cathode electrode revealed noteworthy differences. It was discovered that the cell equipped with an AC cathode MPL (16.696 Ω) exhibited a higher R$_C$ value compared to the cells with KB (13.534 Ω) and AC15% (10.295 Ω) cathode MPL. The result shows that the cell with AC cathode MPL experienced the highest mass transfer resistance. This might be due to the increased presence of micropores (from 15.64% to 27.34%) and the hydrophobic nature of the electrode, as described in the literature [Balakrishnan et al. 2017; Thomas et al. 2019]. Although this improvement enhanced both capillary pressure and water backflow, the dominant effect on mass transfer within the cathode electrode of a passive DEFC was possibly the enhancement of gas permeability. Compared to

passive DMFC, an acid passive DEFC exhibits lower performance due to reduced kinetic reactions on both sides. Additionally, it has been confirmed that the products of the ethanol oxidation reaction are incomplete, leading to a combination of acetaldehyde, acetic acid, and CO_2. This incomplete reaction liberates fewer electrons during transport, typically ranging from only 2 to 4 electrons, causing a decrease in water production at the cathode electrode [An et al. 2015; Badwal et al. 2015]. The presence of sufficient mesopores was believed to facilitate efficient gas transport throughout the cathode electrode. Therefore, a decrease in both mesopores and pore volume, along with increased hydrophobicity within the AC material, could potentially lead to reduced gas permeability, resulting in higher kinetic reaction resistance. On the other hand, the cell equipped with AC15% cathode MPL, the mass transfer resistance was observed to be the lowest. This could be attributed to the presence of an optimal amount of micro/mesopores in the AC15% cathode MPL, which facilitated an optimized gas transfer rate and improved water removal. Nevertheless, other factors could adversely affect the cell performance with an AC15% cathode MPL.

Furthermore, the R_A, which represents the kinetic resistance of the anode reaction, would be the same among the three cells due to their identical anode structure and preparation condition [Cao et al. 2010]. However, the results indicate variations in the R_A among the cells. The cell with a 15% AC cathode MPL exhibited the highest R_A of 1.1972 Ω compared to the cells with KB (0.6262 Ω) and AC (0.4394 Ω) cathode MPL. It was clearly seen that the activation loss of the anode increased significantly by 267% in the cell with an AC15% cathode MPL. To address this inconsistency, further examination was carried out using anode EIS measurements.

In-situ EIS was conducted on the anode half cells using a DHE to study the ohmic and kinetic resistance of the anode electrode. The impedance spectra and its equivalent circuit for the anode half cells were analyzed and are displayed in Figure 8. The chi-square (χ^2) values produced from the simulations ranged from 0.06 to 0.09, and Table 3 shows the fitting parameters. In this case, the physical parameters could be modified based on the previous works [Cao et al. 2010; Cao et al. 2014; Ekdharmasuit et al. 2014]. L, W, and R_{ohm} correspond to the same meanings as in the whole cell experiment. R_1 and R_A represent the contact resistance and kinetic resistance of the anode electrodes, respectively. CPE_1 and CPE_A characterize the capacitive behavior, indicating the roughness and non-uniformity of the membrane-catalyst layer interface and anode electrodes, respectively. The anode ohmic resistance of these three cells was clearly observed to be identical, with a slight variation ranging from 0.47 to 0.55 Ω. Additionally, the contact resistance of the anode electrode, represented by R_1, showed quite similar values ranging from 0.2612 to 0.2693 Ω. This consistency could be attributed to the uniform composition and preparation technique employed for the anode electrodes, which was in agreement with the literature [Cao et al. 2010]. Therefore, it is important to highlight that the unequal ohmic
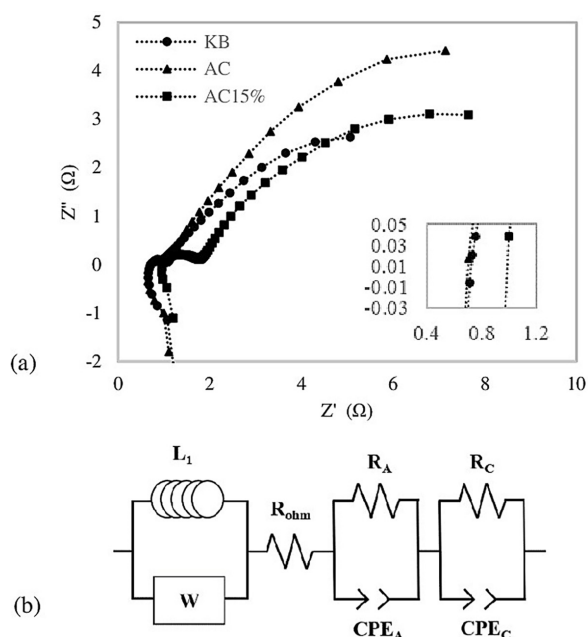

Figure 7. Electrochemical impedance spectra for three passive DEFCs with the AC, AC15% and conventional cathode diffusion layer, respectively, at 4 M ethanol solution and 25 °C (a) and Equivalent circuit for the EIS analysis (b)

Table 2. The obtained fitting parameters for the equivalent circuit model applied to three passive DEFCs with the AC, AC15% and conventional cathode diffusion layer, respectively, at 4 M ethanol solution and 25 °C

Parameter	KB	AC	AC15%
R_{ohm} (ohm)	0.7175	0.6974	0.9818
R_A (ohm)	0.3262	0.4394	1.1972
CPE_A (F)	0.0098	0.0006	0.0026
R_C (ohm)	13.534	16.696	10.295
CPE_C (F)	0.2107	0.1354	0.1150
χ^2	0.0529	0.0426	0.0290

resistance observed in the in-situ EIS analysis of the whole cell, especially in the case of the cell with AC 15% cathode MPL, as discussed earlier, may be primarily influenced by the cathode electrode. Factors such as poor surface contact and the hydrophobic nature resulting from the incorporation of AC into the cathode electrode could impact electronic conductivity, thus diminishing the overall cell performance.

Regarding R_A, which represents the kinetic resistance of the anode electrode, the results indicate that the cell with a AC15% cathode MPL exhibited the highest R_A of 22.33 Ω, while the cells with KB (18.433 Ω) and AC (18.948 Ω) cathode MPL showed similar values. In fact, the kinetic reaction resistance of the anode electrode would be the same among the three cells due to having identical anode structure and conditions. However, in this particular case, it increased slightly by 21% in the cell with a AC15% cathode MPL. Although the effects were not as significant as in the case of the whole cell, which experienced a 267% increase, there were still noticeable impacts on the anode of the cell with an AC15% cathode MPL. It was believed that the characteristics of the cathode electrode might have a slight impact on the kinetic reaction resistance of the anode electrode due to the use of the cathode electrode as a DHE. The
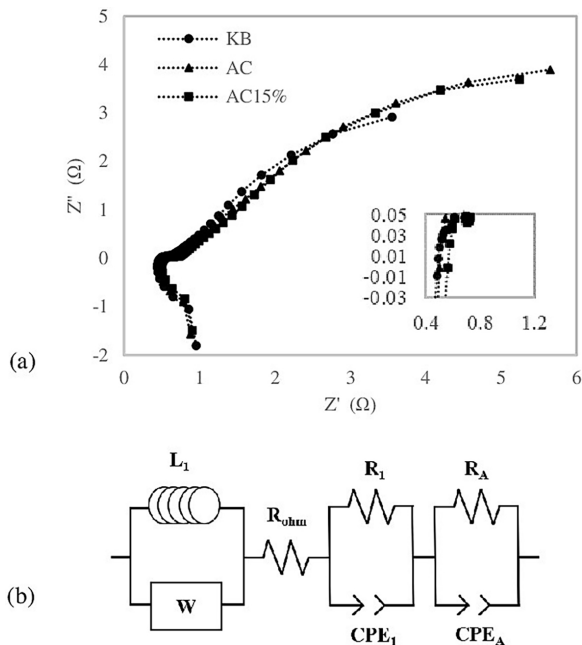
Table 3. The obtained fitting parameters for the equivalent circuit model applied to three anode half-cell with the AC, AC15% and conventional KB cathode diffusion layer, respectively, at 4 M ethanol solution and 25 °C

Parameter	KB	AC	AC15%
R_{ohm} (ohm)	0.4771	0.4997	0.5548
R_1 (ohm)	0.2693	0.2684	0.2612
CPE_1 (F)	0.0939	0.0009	0.0029
R_A (ohm)	18.433	18.948	22.325
CPE_A (F)	0.3170	0.1815	0.2096
x^2	0.0959	0.0653	0.0791

findings reveal that the presence of AC15% cathode electrodes affected the cells not only through the anode kinetics of ethanol oxidation but also due to the electronic conductivity within the cathode electrode. This can confirm the formation of surface cracks, which had a minor influence on the kinetics of the oxidation process of ethanol.

Influence of ethanol concentration on cell performance

By examining the cell polarization at different ethanol concentrations, a correlation between the maximum power density and the ethanol feed concentration was established. This analysis enables to study the behavior of the optimal concentration of ethanol solution, which is illustrated in Figure 9. The results indicate that the performance sequence of the cells remained consistent regardless of the feed concentrations. Certainly, the optimum feed concentration consistently occurred at approximately 4 M for all cells, which concurred with the literature [Shrivastava et al.
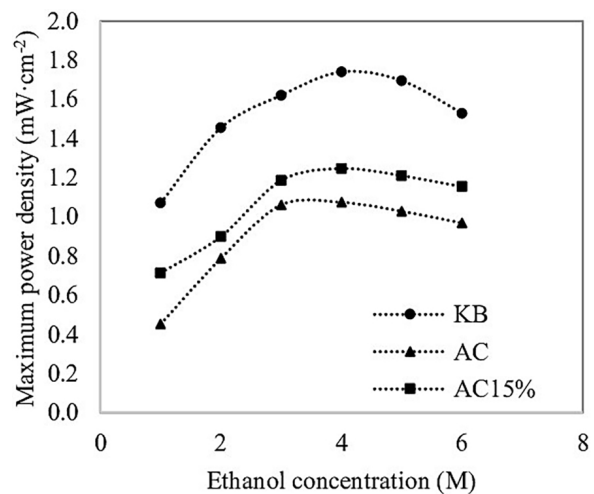
Figure 8. Anode half-cell impedance spectra for three passive DEFCs with the AC, AC15% and conventional KB cathode diffusion layer, respectively, at 4 M ethanol solution and 25 °C (a) and Equivalent circuit for the EIS analysis (b)

Figure 9. Relationship between ethanol concentration and cell maximum power density for all cells

2019]. The performance of the cells improved within the range of dilute ethanol solutions (1–3 M), but declined as the feed concentration exceeded 4 M. The decrease in cell performance at low ethanol concentrations could be attributed to the use of insufficient ethanol molecules for the kinetic reaction rate. Conversely, as the ethanol concentration increases further, the cell performance declined due to the negative effects of ethanol crossover [Ekdharmasuit et al. 2014; Azam et al. 2019; Shrivastava et al. 2019].

To explore the influence of ethanol crossover, the OCVs associated with the ethanol that permeated from the anode to the cathode electrode were analyzed. The OCV was negatively affected by ethanol crossover as a result of the mixed potential at the cathode electrode. The relationship between OCV and ethanol feed concentration is depicted in Figure 10. The results clearly show that increasing ethanol concentration led to a consistent decrease in OCVs for all cells. This decline was due to the enhanced ethanol diffusion and crossover caused by high ethanol concentrations. Notably, the cell using an AC cathode MPL exhibited a higher OCV compared to the others, confirming the hydrophobic nature of the AC cathode MPL and its effective reduction of ethanol crossover. Nevertheless, the cell performance with an AC cathode MPL was not improved, because the electrode possessed unsuitable mesopores and micropores for gas and liquid transport.

Finally, the relationship between the limiting current densities obtained from the anode half-cell polarization measurement for these three cells and different concentrations of ethanol solution is displayed in Figure 11. It was shown that as the ethanol content was raised, the anode limiting current densities for all cells increased but did not reach their maximum levels. When comparing the relationship between ethanol concentration and cell maximum power density for all cells (Figure 9), as well as the relationship between ethanol concentration and anode limiting current density (Figure 11), an interesting observation became apparent. Above an ethanol concentration of 4 M, the trends appear to be opposite. The anode limiting current densities continued to increase, while the cell performances were inhibited with further increases in ethanol concentration. Thus, it could be concluded that higher ethanol concentration reduced cell performance due to the unfavorable effect of ethanol crossover, which affected both the cathode performance and the overall cell performance.
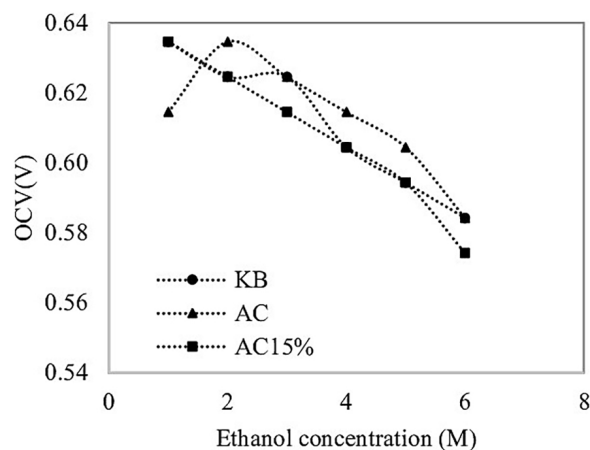

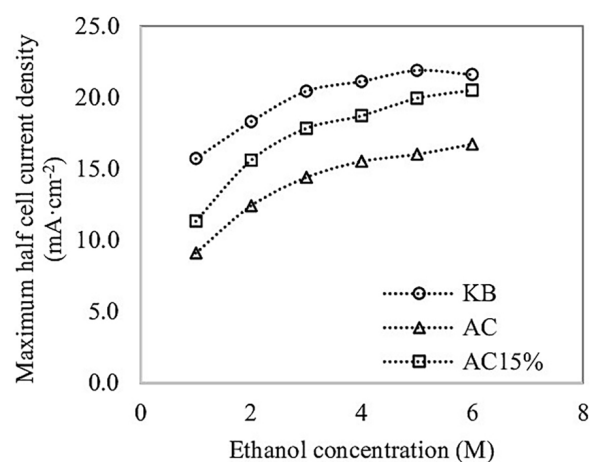**Figure 10.** Relationship between ethanol concentration and cell open circuit voltage for all cells

Figure 11. Relationship between ethanol concentration and anode limiting current density for all cells

CONCLUSIONS

The effects of different cathode MPLs on the performance of passive DEFCs were examined. The cell with a conventional KB cathode MPL exhibited the highest performance, while the cell with an AC cathode MPL showed the lowest performance. The lower pore volume increased micropores, and hydrophobic nature of the AC cathode MPL hindered gas transport and water removal rate. Although mixing AC with KB in the cathode MPL improved the proportion of micropores and mesopores, the heterogeneous contact surface between the cathode catalyst layer and the cathode MPL, which causes a larger ohmic resistance, prevented the performance of the cell with AC15% cathode MPL from being improved. However, incorporating biomass-based materials in the electrode could be an interesting approach, as it allows for low-cost production

using inexpensive carbon precursors. A systematic study of durian shell activated carbons could yield carbon materials with better properties for MPLs in passive DEFCs. Optimizing water removal rate, gas transport channels, and electronic conductivity will be crucial for achieving a promising cathode MPL in DEFCs.

Acknowledgements

REFERENCES

1. An L., Zhao T.S., Li Y.S. 2015. Carbon-neutral sustainable energy technology: Direct ethanol fuel cells. Renewable and Sustainable Energy Reviews, 50, 1462–1468.

2. Azam A.M.I.N., Lee S.H., Masdar M.S., Zainoodin A.M., Kamarudin S.K. 2019. Parametric study on direct ethanol fuel cell (DEFC) performance and fuel crossover. International Journal of Hydrogen Energy, 44(16), 8566–8574.

3. Badwal S.P.S., Giddey S., Kulkarni A., Goel J., Basu S. 2015. Direct ethanol fuel cells for transport and stationary applications – A comprehensive review. Applied Energy, 145, 80–103.

4. Balakrishnan P., Inal I.G., Cooksey E., Banford A., Aktas Z., Holmes S.M. 2017. Enhanced performance based on a hybrid cathode backing layer using a biomass derived activated carbon framework for methanol fuel cells. Electrochimica Acta, 251, 51–59.

5. Braz BA., Oliveira V.B., Pinto A.M.F.R. 2019. Experimental studies of the effect of cathode diffusion layer properties on a passive direct methanol fuel cell power output. International Journal of Hydrogen Energy, 44(35), 19334–19343.

6. Cao J., Chen M., Chen J., Wang S., Zou Z., Li Z., et al. 2010. Double microporous layer cathode for membrane electrode assembly of passive direct methanol fuel cells. International Journal of Hydrogen Energy, 35, 4622–4629.

7. Cao J., Wang L., Song L., Xu J., Wang H., Chen Z., et al. 2014. Novel cathodal diffusion layer with mesoporous carbon for the passive direct methanol fuel cell. Electrochimica Acta, 118, 163–168.

8. Ekdharmasuit P., Therdthianwong A., Therdthianwong S. 2013. Anode structure design for generating high stable power output for direct ethanol fuel cells. Fuel, 113, 69–76.

9. Ekdharmasuit P., Therdthianwong A., Therdthianwong S. 2014. The role of an anode microporous layer in direct ethanol fuel cells at different ethanol concentrations. International Journal of Hydrogen Energy, 39, 1775–1782.

10. Elsaid K., Abdelfatah S., Elabsir A.M.A., Hassiba R.J., Ghouri Z.K., Vechot L. 2021. Direct alcohol fuel cells: Assessment of the fuel's safety and health aspects. International Journal of Hydrogen Energy, 46(59), 30658–30668.

11. Hiramitsu Y., Sato H., Hori M. 2010. Prevention of the water flooding by micronizing the pore structure of gas diffusion layer for polymer electrolyte fuel cell. Journal of Power Sources, 195, 5543–5549.

12. Matos B.R., Goulart C.A., Tosco B., da Silva J.S., Isidoro R.A., Santiago E.I., et al. 2020. Properties and DEFC tests of Nafion - Functionalized titanate nanotubes composite membranes prepared by melt-extrusion, 604, 118042.

13. Monreal J.S., García-Salaberri P.A., Vera M. 2019. A mathematical model for direct ethanol fuel cells based on detailed ethanol electro-oxidation kinetics. Applied Energy, 251, 113264.

14. Moreno-Jiménez, D.A., Pacheco-Catalán D.E., Ordóñez L.C. 2015. Influence of MEA Catalytic Layer Location and Air Supply on Open-Cathode Direct Ethanol Fuel Cell Performance. International Journal of Electrochemical Science, 10(11), 8808–8822.

15. Oliveira V.B., Pereira J.P., Pinto A.M.F.R. 2017. Modeling of passive direct ethanol fuel cells. Energy, 133, 652–665.

16. Ong B.C., Kamarudin S.K., Basri S. 2017. Direct liquid fuel cells: A review. International Journal of Hydrogen Energy, 42 (15), 10142–10157.

17. Pereira J.P., Falcão D.S., Oliveira V.B., Pinto A.M.F.R. 2014. Performance of a passive direct ethanol fuel cell. Journal of Power Sources, 256, 14–19.

18. Pittayaporn N., Therdthianwong A., Therdthianwong S., Songprakorp R. 2019. Dynamic modeling of direct ethanol fuel cells upon electrical load change. International Journal of Energy Research, 43(7), 2615–2634.

19. Prabhuram J., Krishnan N.N., Choi B., Lim T.H., Ha H.Y., Kim S.K. 2010. Long-term durability test for direct methanol fuel cell made of hydrocarbon membrane. International Journal of Hydrogen Energy, 35, 6924–6933.

20. Shaari N., Kamarudin S.K., Bahru R., Osman S.H., Ishak N.A.I.M. 2020. Progress and challenges: Review for direct liquid fuel cell. International Journal of Energy Research, 45, 6644–6688.

21. Shrivastava N.K., Chadge R.B., Ahire P., Giri J.P. 2019. Experimental investigation of a passive direct ethanol fuel cell. Ionics, 25, 719–726.

22. Tey J.P., Careem M.A., Yarmo M.A., Arof A.K. 2016. Durian shell-based activated carbon electrode for EDLCs. Ionics, 22, 1209–1216.

23. Thomas P., Lai C.W., Johan M.R.B. 2019. Recent developments in biomass-derived carbon as a potential sustainable material for super-capacitor-based energy storage and environmental applications. Journal of Analytical and Applied Pyrolysis, 140, 54–85.

24. Wang K., Wang F., Zhao Y., Zhang W. 2021. Surface-tailored PtPdCu ultrathin nanowires as advanced electrocatalysts for ethanol oxidation and oxygen reduction reaction in direct ethanol fuel cell. Journal of Energy Chemistry, 52, 251–261.

25. Weber A.Z., Newman J. 2005. Effects of Microporous Layers in Polymer Electrolyte Fuel Cells. Journal of The Electrochemical Society, 152, A677–A688.

26. Yong Y.W., Azam A.M.I.N., Masdar M.S., Zainoodin A.M., Kamarudin S.K. 2020. Anode structure with double-catalyst layers for improving the direct ethanol fuel cell performance. International Journal of Hydrogen Energy, 45(42), 22302–22314.

27. Zhang J., Feng L., Cai W., Liu C., Xing W. 2011. The function of hydrophobic cathodic backing layers for high energy passive direct methanol fuel cell. Journal of Power Sources, 196, 9510–9515.